Synthesis and characterization of metal oxide-based microcapsules including phase change materials for energy storage applications

T. Aguilar[1] · M. D. Peña-Cordero[1] · I. Carrillo-Berdugo[1] · R. Alcántara[1] · J. Navas[1]

Abstract

In this study, microcapsules based on Cu_2O containing different phase change materials (PCM) were prepared and characterized. The elemental, structural and electronic properties of the Cu_2O-based microcapsules were characterized using several techniques such as X-ray diffraction, X-ray photoelectron spectroscopy, scanning and transmission electron microscopy and Fourier-transform infrared spectroscopy. In addition, the thermal properties of the microcapsules prepared were characterized in order to analyse their possible application as a thermal energy storage medium. Heating/cooling cycles using a differential scanning calorimetry technique were performed, and the phase change temperature and enthalpy were estimated. We observed good stability after the cycles. Furthermore, the encapsulation efficiency was estimated from melting and crystallization enthalpy values, reaching a value of 14.8% for the paraffin wax-based microcapsules. Finally, isobaric specific heat was measured to evaluate the storage capability of the encapsulated PCMs with regard to pure Cu_2O to evaluate their possible application as a thermal storage system. An increase of around 140% was found in the isobaric specific heat for the microcapsules based on paraffin wax with regard to pure Cu_2O.

Introduction

Nowadays, the energy crisis, increasing pollution and the climate change are big problems for our society which have to be addressed in the near future. World energy consumption continues to grow, which results in the extraordinarily high use of non-renewable fossil fuels, which are the main source of CO_2 emissions. Thus, scientists have focussed a great deal of research on the development of new methods for the production, conversion and storage of energy [1]. In recent decades, several renewable energy sources have been studied for energy production, but these are usually intermittent sources, which is a significant problem for their implementation. For this reason, energy storage technologies are currently being studied, one that stands out being the use of phase change materials (PCM) for storing thermal energy, which is found as latent heat in the bonds of the materials [2]. In this sense, PCMs have been proven to be promising for use in a range of application: solar heating systems or in industrial waste heat [3]; cold thermal energy storage [4]; domestic heating/cooling [5]; or in parabolic trough collectors for direct steam generation [6].

In addition, they can be applied in building materials, where PCMs are capable of capturing and releasing large amounts of energy during melting and solidification at specific temperatures, so there is an increase in the use of thermal energy because the mismatch between energy supply and demand is reduced [7]. According to the nature of the PCM, the process can be defined as solid–solid, solid–liquid, liquid–gas or solid–gas energy storage. However, in building materials, the phase changes involving a gas phase cannot be applied due to the significant change in volume and pressure. Moreover, solid–solid PCMs store the energy in the crystalline structure changes, which typically is lower than for other phase change processes, but some novel studies is being reported for example based on solvent-free radical polymerization of methyl methacrylate with methacrylate-functionalized polyethylene glycol (PEG) [8]. Therefore, the solid–liquid PCMs are the most extended for use in building

✉ T. Aguilar
mariateresa.aguilar@uca.es

✉ J. Navas
javier.navas@uca.es

1 Departamento de Química Física, Facultad de Ciencias, Universidad de Cádiz, 11510 Puerto Real (Cádiz), Spain

Table 1 Microcapsules synthesized and PCMs used, including the melting and reaction temperature

Sample	PCM	T_m/K	T_r/K
Cu$_2$O@C14	n–tetradecane	278.9	323
Cu$_2$O@C18	n–octadecane	299–302	323
Cu$_2$O@PW	Paraffin wax	323–330	353
Cu$_2$O-Ref	–	–	323

materials. Some inorganic materials have been tested, such as sodium sulphate decahydrate [9], or sodium sulphate encapsulated with methyl methacrylate [10]. In this sense, organic PCMs such as paraffin and fatty acids show interesting properties but they could leak into the surroundings during the heat storage process, besides being flammable, which implies serious potential fire risk. These problems can be addressed by using encapsulation technology to produce microencapsulated or nanoencapsulated PCMs [7].

For encapsulation, several materials have been used in the shell. Several studies have reported the successful use of polymers: Docosane loaded capsules using polyurethane as shell material have been reported [11]; and inorganic shells with organic PCMs, such as SiO$_2$ encapsulating stearic acid [12], paraffin wax [13] or n-octadecane [14], or CuO loaded with palmitic acid [15]. In addition, C-based materials such as graphene oxide [16] or carbon nanotubes have been used as the shell [17], for example Wu et al. reported the encapsulation of lauric acid in carbon nanotubes [18], and Meng et al. reported the preparation of composites based on carbon nanotubes and fatty acids as phase change materials [19].

Therefore, in this study organic paraffin PCMs were encapsulated. Paraffins are safe, reliable, cheap, non-corrosive and have low vapour pressure, making them good candidates for encapsulation [11]. n-tetradecane (C14), n-octadecane (C18) and paraffin wax (a mixture of hydrocarbons) were used as the encapsulated core material, using copper oxide (Cu$_2$O) as the encapsulating material. Cu$_2$O was chosen because it is a typical p type semiconductive material which has attracted an intense interest for its various characteristic properties in recent years. It has obtained wide applications for solar photocatalysis, photoelectrolytic cells, antifouling coatings,… And also, Cu$_2$O is especially characteristic for its low toxicity and good environmental acceptability [20]. The capsules were characterized for their physical and chemical properties by means of X-ray diffraction, electron microscopy, Fourier-transform infrared spectroscopy and X-ray photoelectron spectroscopy. Their thermal properties were characterized using differential scanning calorimetry, obtaining the melting and solidification temperature and enthalpy. Moreover, the stability of the capsules prepared was analysed by developing heating/cooling cycles.
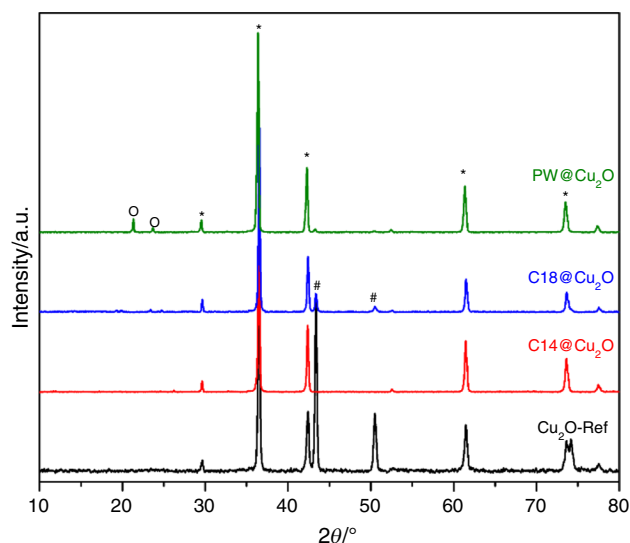
Fig. 1 XRD patterns of synthesized samples, where * corresponds to Cu$_2$O, # to metallic Cu, and ° to paraffin wax

Experimental section

Preparation of microcapsules

Cu$_2$O@PCM microcapsules were synthesized by means of an in situ precipitation method. The reaction was performed in a 500 mL three-neck round-bottom flask on a hot plate stirrer equipped with a heat-on system. To avoid evaporation of the water, the reaction was performed under reflux. The synthesis involved four steps: (i) preparation of water/PCM emulsion, (ii) cation covering, (iii) reduction and (iv) ageing. To prepare the emulsion, cetyltrimethylammonium bromide (CTAB, purity ≥ 99%, Sigma-Aldrich©) was used as a surfactant. A total of 4.80 g of the phase change material (PCM), 4.66 g of CTAB and 80 mL of water were added to a three-neck round-bottom flask on a hot plate stirrer equipped with a heat-on system. Table 1 shows the PCMs used and the name given to each sample. The mixture was kept under constant stirring for 1.5 h at the reaction temperature (T_r) detailed in Table 1 for each PCM. During this process, a white emulsion was observed. After the emulsion preparation, 60 mL of Cu$_2$SO$_4$ solution (0.02 M) was added at a rate of 2.4 mL min^{-1}. Then, the mixture was kept at the same temperature for 4 h to ensure the complete covering of the micelle formed by Cu^{2+}, observing a colour change to turquoise blue. The next step was the Cu^{2+} reduction to obtain copper oxide. For this, 100 mL of a solution of NaOH (5 M) and 60 mL of a glucose solution (0.28 M) were added dropwise simultaneously. The reaction was kept under stirring at the same temperature for 6 h, and a brick red solid in suspension was obtained. Finally, the suspension was kept
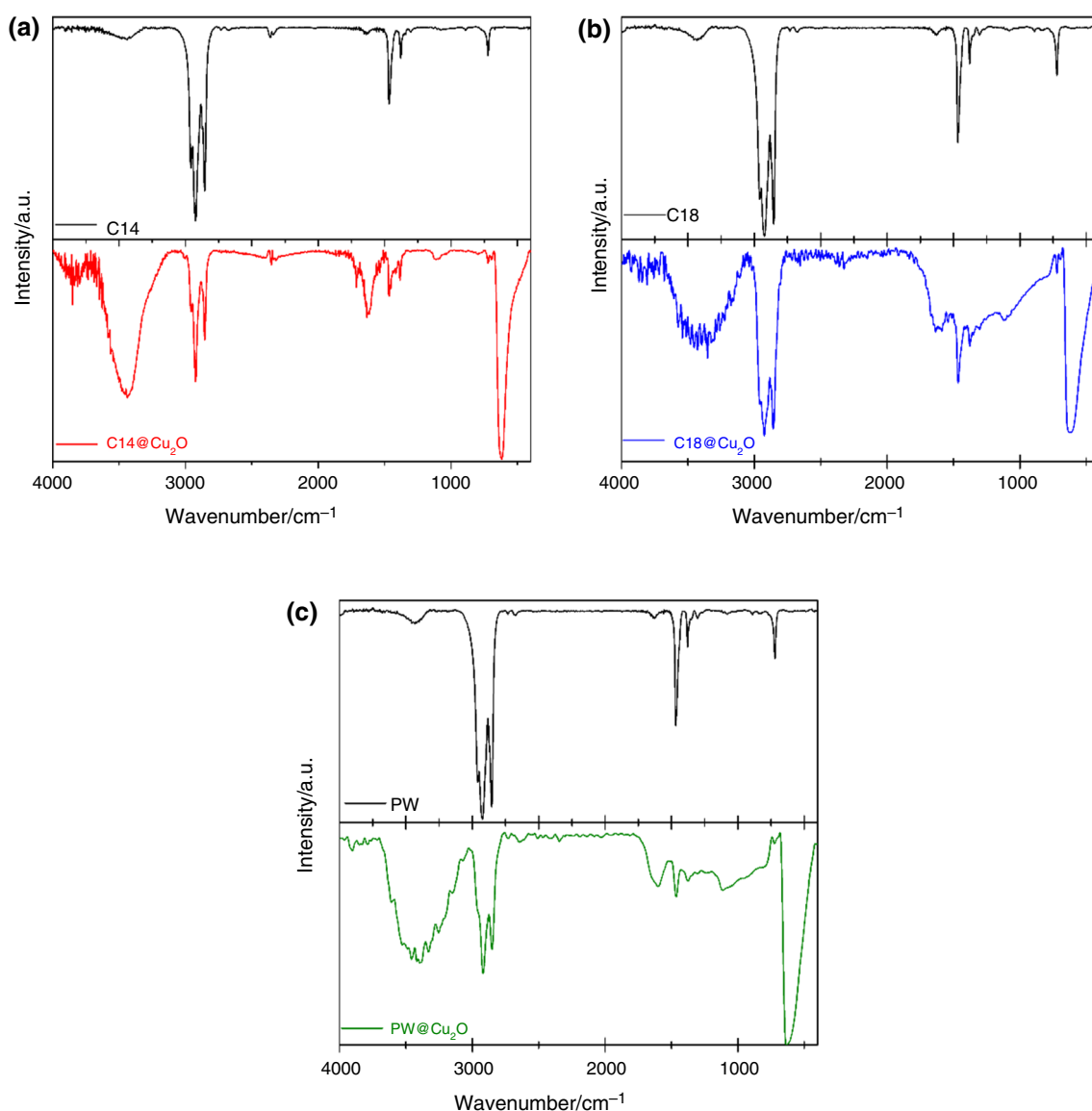
Fig. 2 FTIR spectra of synthesized samples and pure PCMs: **A** C14 and $Cu_2O@C14$, **B** C18 and $Cu_2O@C18$ and **C** PW and $Cu_2O@PW$

at the same temperature without stirring and reflux for 10 h for the complete formation of the Cu_2O structure.

A Cu_2O reference sample was synthesised using the same procedure but without adding the PCM.

Characterization of microcapsules

Several techniques were used to observe the formation of microcapsules and to determine the structure and morphology of the synthesized material. Crystalline phases present in the microcapsules were determined using X-ray diffraction (XRD) (Bruker®, D8 Advance A25 diffractometer) with Cu-Kα radiation with a wavelength of 1.5406 Å and a Lynxeye detector. The samples were measured in a 2θ range from 10° to 80° with an accuracy of 0.020°/step, taken at

40.0 kV and 40.0 mA. Fourier-transform infrared (FTIR) spectroscopy was performed to characterize the chemical structures of the microcapsules on a Bruker® spectrometer, model Tensor37. The spectra were recorded from 400 to 4000 cm^{-1} and at a resolution of 2 cm^{-1}. In addition, the oxidation state and chemical state bonding of the elements were analysed using a Kratos® spectrometer, model Axis UltraDLD, equipped with monochromatized Al Kα radiation (1486.6 eV) and a passage energy of 20 eV and an accuracy of 0.1 eV. The peak at 284.8 eV corresponding to the C 1 s signal was used as a reference for the binding energy scale. The morphology and size distribution of the microcapsules and Cu_2O particles were both studied by means of scanning (SEM) and transmission electron microscopy (TEM). A Nova NanoSEM 450 microscope and a Talos F200X

microscope, both supplied by FEI®, were employed for the scanning and transmission electron microscopy, respectively. In addition, energy-dispersive X-ray spectroscopy (EDX) was performed in the transmission electron microscopy technique to analyse the elemental composition of the samples.

Thermal characterization was performed by means of the values for the sensible and latent heat of the Cu_2O microcapsules using a DSC 214 Polyma supplied by Netzsch®. The heat capacity of the samples was analysed using the temperature modulated differential scanning calorimeter (TM-DSC) technique in the temperature range established according to the working temperature of each PCM. The latent heat was estimated by DSC. The established programmes are detailed in the Supplementary Information for each sample. The thermal and chemical stability of the pure PCMs and microcapsules were also analysed after ten and thirty cycles, respectively.

Results and discussion

Structural and morphological characterization

Figure 1 shows XRD diffractograms corresponding to the synthesized microcapsules and Cu_2O powder. The patterns obtained for all the samples show peaks at $2\theta = 29.7º$, 36.5º, 42.4º 61.5º, 73.9º and 77.0º. These peaks are in agreement with the reference pattern of Cu_2O with a cubic crystalline structure and Pn-3 m space group, and can be assigned to the reflection of the (111), (200), (110), (220), (311) and (222) planes, respectively. Also, a cubic crystalline structure (Fm-3 m space group) of metallic copper can be observed in all the samples, except in the capsules including C14 inside, i.e. $Cu_2O@C14$. But the amount of metallic Cu is higher in the Cu_2O sample without PCM used as reference, which means that the synthesis developed leads to the production of a certain amount of metallic Cu. Therefore, the formation of the microcapsules using PCMs leads to a decrease in the formation of metallic Cu. Finally, the sample $Cu_2O@$ PW shows two sharp diffraction peaks at $2\theta = 21.6°$ and $2\theta = 24.0°$, the typical diffractions of the (110) and (200) crystal planes of monoclinic paraffin, respectively. The diffractogram for the paraffin wax was measured for comparison with the synthesized microcapsules and is included in Figure S1 in the Supplementary Information.

Figure 2 shows the FTIR spectra of the synthesized microcapsules and the pure PCMs. All the microcapsule samples show three absorption peaks in the infrared spectra between 2750 and 3150 cm^{-1}, which are assigned to C–H stretching, and are typical for hydrocarbon compounds. It is also possible to observe two peaks at 1471 and 1365 cm^{-1} and one at 717 cm^{-1} corresponding to the C–H bending vibrations and the C–H deformation vibration, respectively.
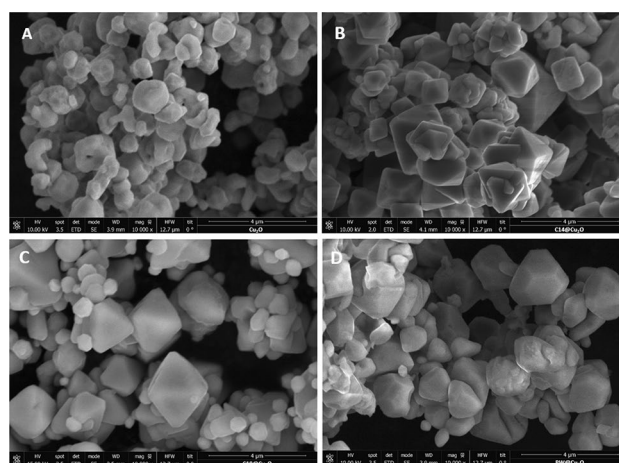
**Fig. 3** SEM images of **A** Cu_2O, **B** $C14@Cu_2O$, **C** $C18@Cu_2O$ and **D** $PW@Cu_2O$

These are characteristic peaks of the pure PCMs used as the core in the microcapsules, as is also observed in the spectra for the pure PCMs shown in Fig. 2. Hence, these peaks are useful to identify the presence of PCM within the synthesized microcapsules. Meanwhile, a characteristic absorption peak at 628 cm^{-1} was obtained for all the synthesized microcapsules. This peak is assigned to the stretching frequency of Cu–O [21], demonstrating the existence of Cu_2O in the microcapsules. This peak is also observed in the Cu_2O sample used as the reference, as Figure S2 in the Supplementary Information shows. Finally, in the synthesized microcapsules and the Cu_2O, it is possible to observe a broad band in the region between 3200 and 3600 cm^{-1}, which can be attributed to absorbed water on the surface of the particles, since this coincides with the vibration band of the O–H bonds. Therefore, thanks to the comparison of the synthesized microcapsules and the PCMs, it could be assumed that there are *n*-tetradecane, *n*-octadecane and paraffin encapsulated with Cu_2O.

Figure 3 shows the SEM images of the Cu_2O (Fig. 3A) and $Cu_2O@PCM$ microcapsules (Fig. 3B–D). Figure 3A shows the Cu_2O nanoparticles, to which neither PCM nor surfactant has been added. The formation process of the microcapsules takes place by the growth of Cu_2O on the micelle containing the PCM, resulting in an octahedral morphology structure. Although the process is common in all cases, by comparing Fig. 3B–D, it can be observed how, due to the PCM having a longer carbon chain, the octahedron seems to be increasingly irregular and its vertices and edges truncated. This may be due to the fact that, as the carbon chain is longer, the micelles that are formed are larger, and it would take more time to age to obtain a regular octahedron. To further confirm the formation of microcapsules, Fig. 4 shows SEM images where it is possible to observe damaged structures, that is broken microcapsules, for samples C18@
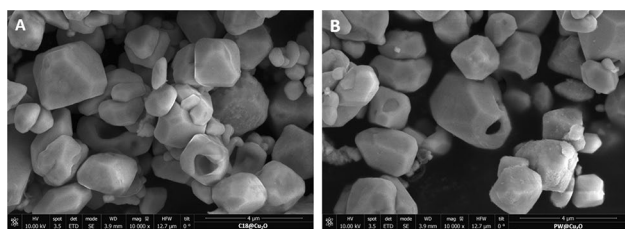
Fig. 4 SEM images of **A** C18@Cu$_2$O and **B** PW@Cu$_2$O, where broken capsules are observed

Cu$_2$O (Fig. 4A) and PW@Cu$_2$O (Fig. 4B). It is interesting to note that the uncompleted formation of microcapsules could be due to unoptimized synthesis conditions. However, these results indicate that *n*-octadecane has been successfully encapsulated into Cu$_2$O by means of an in situ precipitation, followed by a soft reduction with glucose.

Figure 5 shows the TEM analysis performed for the microcapsule samples. The HAADF-TEM investigation also confirms the octahedral shell structure for the microcapsules synthesized using C14 (Fig. 5A) as the core and the irregular morphology for the capsules with C18 and PW (Fig. 5B, C). The three microcapsules samples were also analysed by

EDX. The presence of Cu and O is confirmed, and also the presence of C from the PCMs in the same region of Cu and O, so we can conclude that the PCMs were confined in the Cu$_2$O capsules because no evidence of the PCMS out of the microcapsules was observed in the SEM and TEM images. Figure 6 shows TEM analysis for the Cu$_2$O sample used as a reference. The morphology of the sample is clearly different to that observed for the microcapsules. The EDX analysis only shows the presence of Cu and O, and no evidence of the presence of C, as is observed in Figs. 6B, C.

XP spectra were recorded to analyse the oxidation state and the chemical state bonding of the elements in the three Cu$_2$O-based microcapsule samples. The reference sample of synthesized Cu$_2$O was also measured for comparison purposes. Thus, Figure S3 shows the survey spectra for the four samples and the assignation of the main peaks observed. As expected, the presence of Cu, O and C was confirmed and the shape for the four surveys spectra is quite similar. In addition, Fig. 7A shows the Cu 2p region for the four samples, which are quite similar in all cases. The contribution for Cu 2p$_{3/2}$ appears at a binding energy (BE) of about 933 eV, which is a typical value for Cu(I) [22]. Moreover, the Cu 2p signal shows a significant spin–orbit splitting of
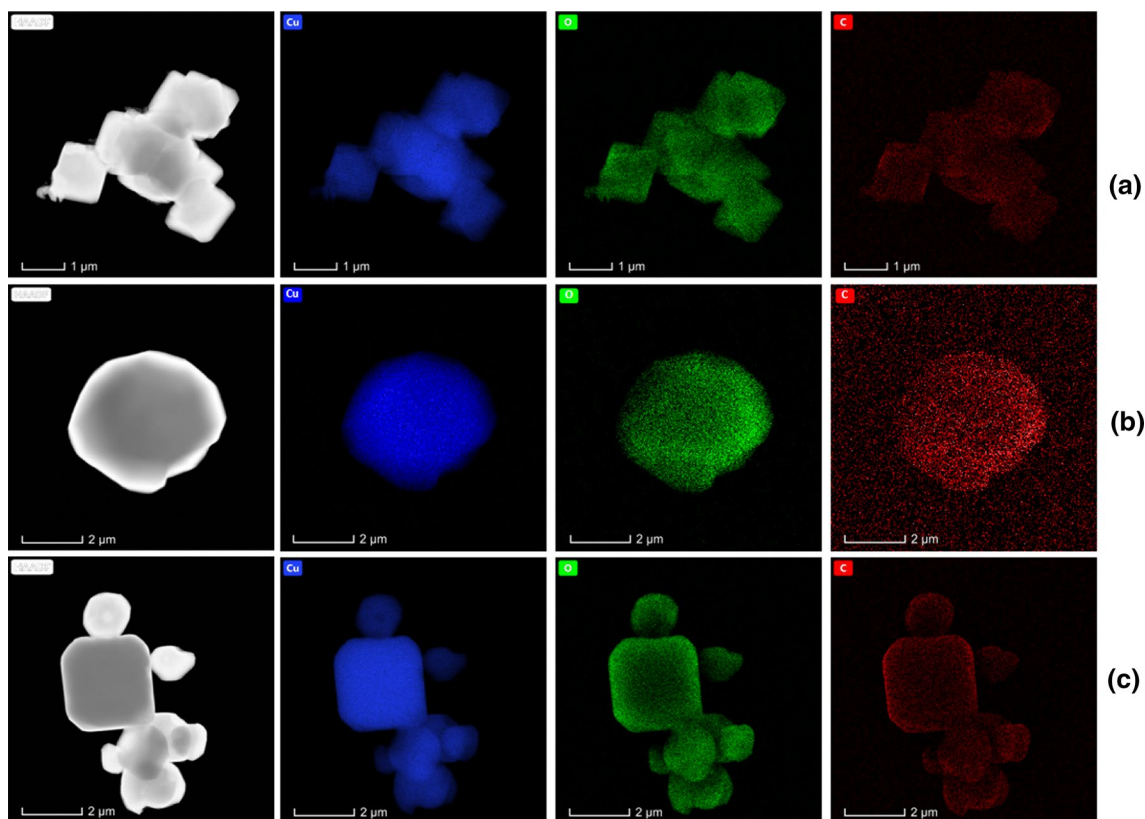
Fig. 5 HAADF-STEM images and EDX mapping of **A** C14@Cu$_2$O, **B** C18@Cu$_2$O and **C** PW@Cu$_2$O. Elemental mapping for copper (blue), oxygen (green) and carbon (red). (Color figure online)

Fig. 6 **A** TEM image, **B** EDX spectrum and **C** HAADF-STEM images of Cu$_2$O-ref and the elemental mapping of Cu (blue) and O (green). (Color figure online)
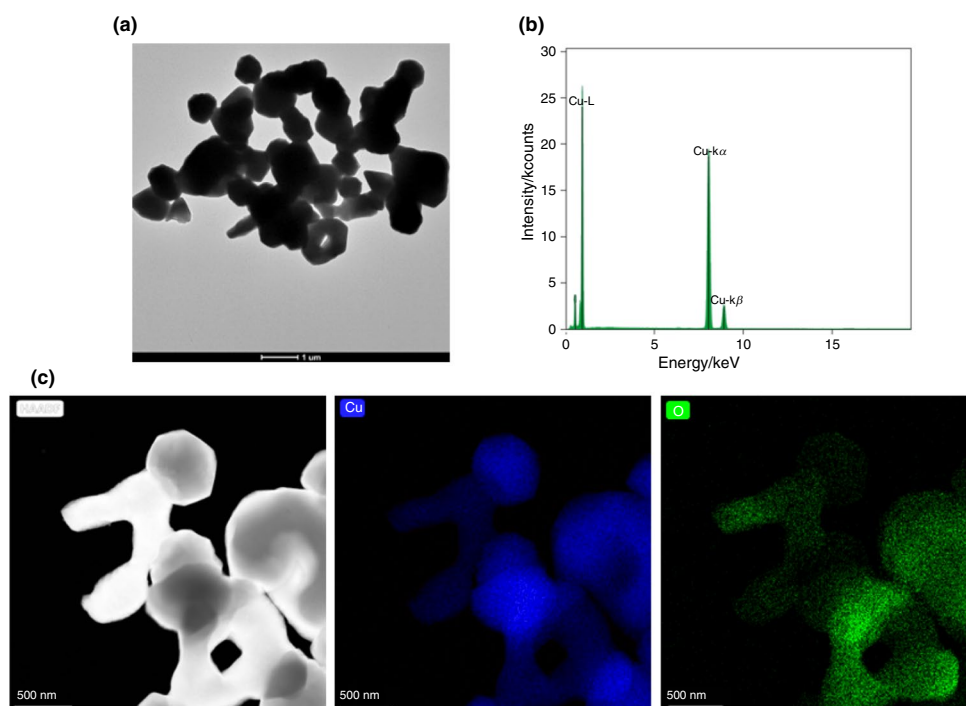

about 19.8 eV. However, the most typical way to distinguish the different oxidation states for Cu from the Cu 2p signal is the presence of satellites features, which are typically very strong for Cu(II), weak for Cu(I) and they are not observed for Cu(0). For the samples analysed, the satellites features are observed but they are weak, so the presence of Cu(I) is confirmed. In addition, the Cu LMM signal can be used to identify the oxidation state, because bigger peak shifts are observed for Cu LMM compared to the Cu 2p signal. Figure 7b shows the Cu LMM region for the four samples. The signal is quite similar in all cases, and they appear at a kinetic energy of about 916.8 eV, which is typical for Cu(I) [22]. Moreover, Fig. 7c shows the signal recorded for the O 1 s region. Again, the signals for all the samples are similar. The peak is observed at about 530.6 eV, which can be assigned to O^{2-} in the lattice of the Cu$_2$O [23], which is coherent with the results shown for the other regions of the XP spectra. This confirms the majority presence of Cu$_2$O in the samples synthesized, as was shown by the XRD results. Finally, Fig. 7d shows the valence band region for the samples. In all cases, the Fermi level is close to 0 eV; thus, the Cu$_2$O-based microcapsules are able to absorb light in a wide range of the electromagnetic spectrum, which is an interesting feature for its application.

Thermal characterization

The microcapsules prepared are intended for use in energy storage, so their thermal characterization is of great interest. To know the enthalpy and temperature of the phase change,

and also the thermal stability is mandatory. Thus, using the programme for DSC measurements shown in the Supplementary Information, this analysis was performed. Figures 8, 9 and 10 show several cycles for the pure PCMs (in Figs. 8a, 9a and 10a for C14, C18 and paraffin wax, respectively) and for the microcapsules prepared (see Figs. 8b, 9b, and 10b for C14@Cu$_2$O, C18@Cu$_2$O, PW@Cu$_2$O, respectively). For the three pure PCMs and for C14@Cu$_2$O, 10 cycles were performed, whereas for the microcapsules C18@Cu$_2$O and PW@Cu$_2$O, 30 cycles were performed. Due to the phase change temperature for C14, only 10 cycles were performed because its application is more limited. The values for melting and solidification enthalpy were estimated from the area under the peak for the endo- and exothermic processes. The melting and crystallization temperatures were estimated from the tangent line of the onset temperature.

The profiles of the DSC plots are similar between the pure PCM and its corresponding microcapsule. The microcapsule samples are powder, so the presence of the phase change peaks in the plots is evidence of the formation of the capsules including the PCMs inside. From these profiles, the melting and crystallization temperature have been estimated, and the values are shown in Fig. 11. In the case of the C14-based microcapsules, the melting and crystallization temperatures are in the range of 274–278 K, as is expected. The melting point is higher than the solidification point, which also occurs for C18 and PW. The crystallization temperature for the microcapsules is higher than for C14, which is not so clear for the melting temperatures. For C18, the melting and crystallization temperature for the PCM-based
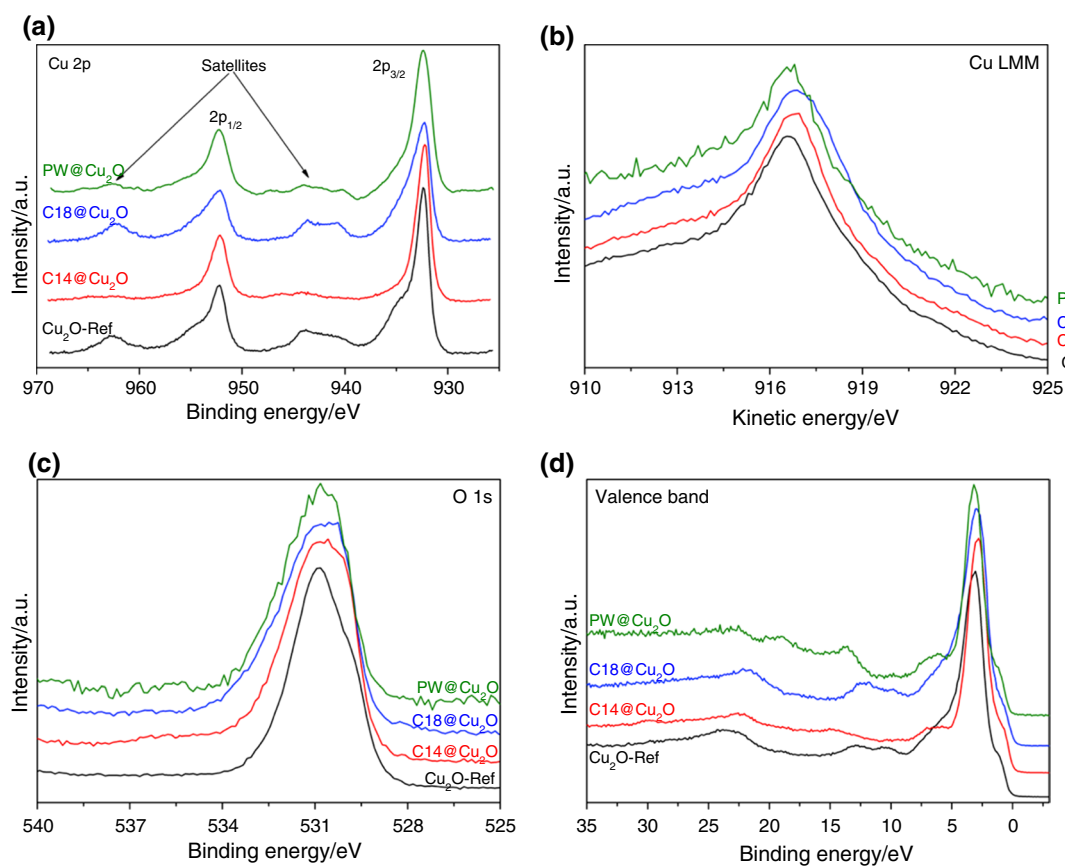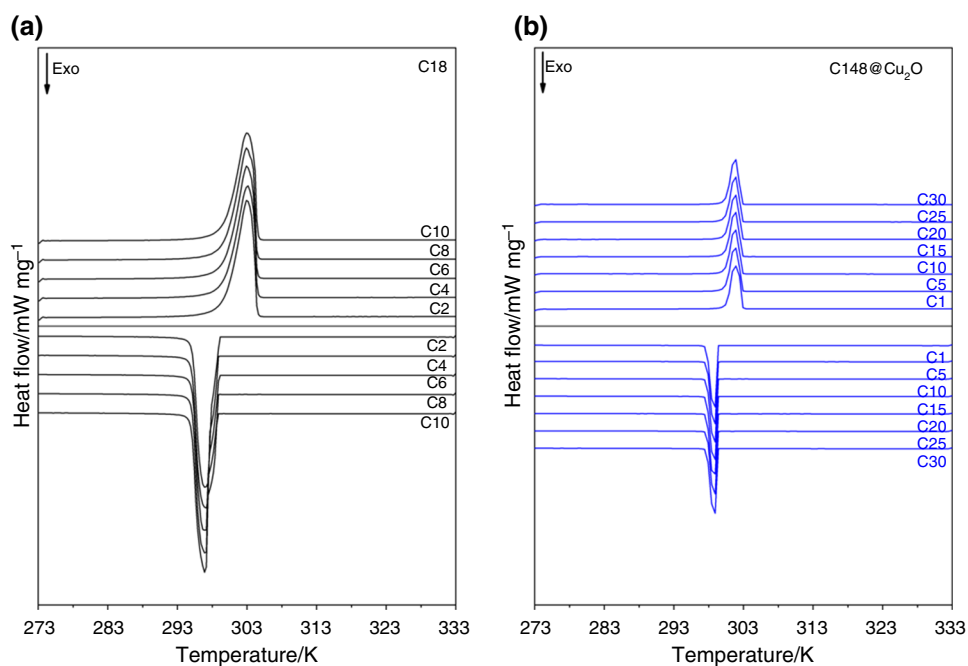
Fig. 7 High resolution XP spectra for the Cu_2O-based microcapsules and Cu_2O reference sample for **a** Cu 2p, **b** Cu LMM, **c** O 1 s and **d** valence band regions
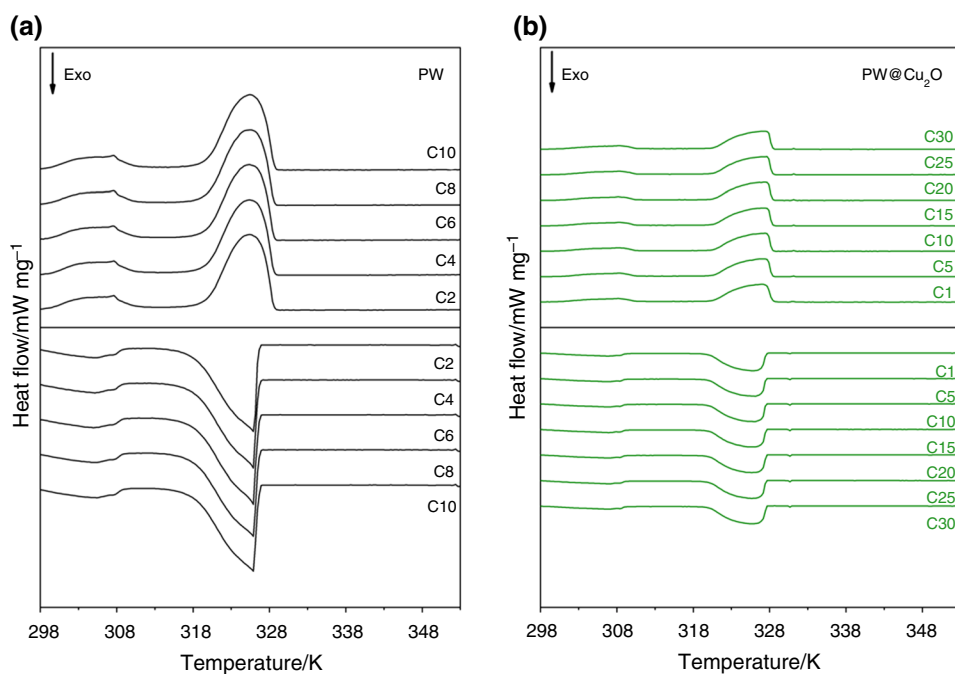
Fig. 8 DSC plots for **a** pure C14 and **b** C14@Cu_2O microcapsules for up to 10 cycles
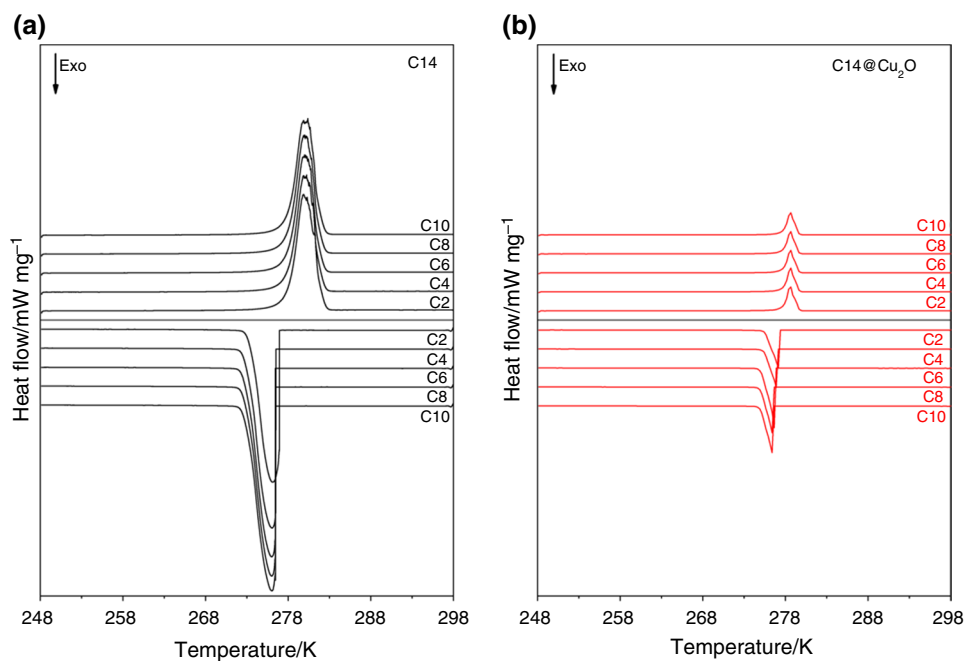
**Fig. 9** DSC plots for **a** pure C18 and **b** C18@Cu₂O microcapsules for up to 10 and 30 cycles, respectively

Fig. 10 DSC plots for **a** pure PW and **b** PW@Cu₂O microcapsules for up to 10 and 30 cycles, respectively

microcapsules are higher than for the pure PCMs. The values observed are between 297 and 301 K. In the case of PW, two melting and crystallization points are observed, first between 318 and 328 K, and second between approximately 295–308 K. This is due to the hydrocarbon composition of the paraffin wax. The values in all cases for the paraffin wax-based microcapsules are slightly higher than for pure the

PW. Therefore, we can observe the presence of the effects of Cu₂O, as is observed in the crystallization temperature, which is higher for the encapsulated PCMs. The melting temperature of the C18 and paraffin wax is higher for the PCM-based microcapsules. In addition, we observe that the values are highly stable in all the cycles. The highest variations are found in the melting point values.
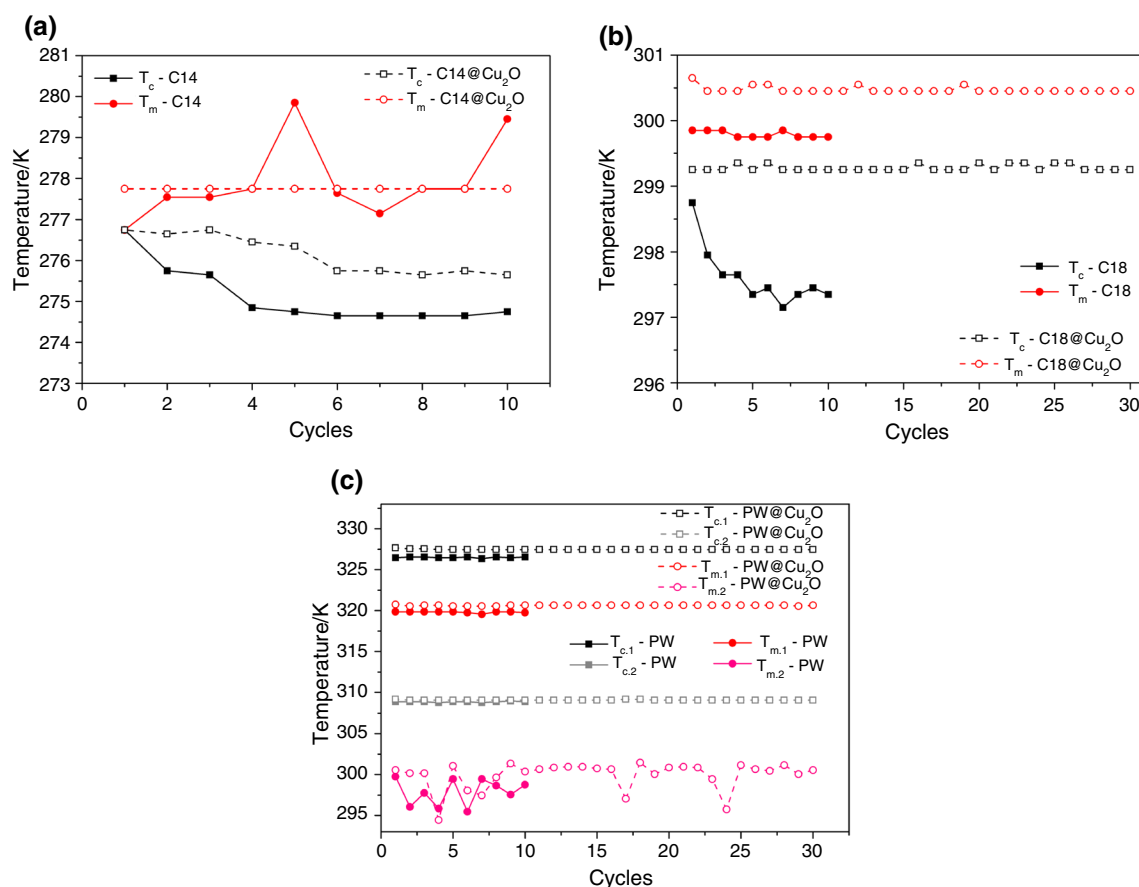
Fig. 11 Crystallization and melting temperatures of the PCMs and the PCMs-based microcapsules for each cycle: **a** C14 and C14@Cu$_2$O, **b** C18 and C18@Cu$_2$O and **c** PW and PW@Cu$_2$O

Melting and crystallization enthalpy were estimated from the DSC plots shown in Figs. 8–10. The results obtained for C14 and the C14-based microcapsules (C14@Cu$_2$O sample) are shown in Fig. 12a. The melting enthalpy for pure C14 was found to be about 210 J g^{-1}, which is coherent with values reported in the literature [24]. The value for the microcapsules is 19 J g^{-1} lower. Moreover, this effect is observed for the other PCMs used. This is coherent due to the lower amount of PCM in the capsule samples with regard to the pure PCM because the mass of the samples used in the DSC measurements is similar, and the capsules include a portion of Cu$_2$O. But also, when PCMs are confined, as in the microcapsules, the configuration of the molecules when they crystalize changes, as does the energy involved in the transition [25]. From the enthalpy values of the melting and crystallization processes, the encapsulation efficiency, φ, can be estimated as $\varphi = 100 \cdot \left[\left(\Delta H_{c,cap} + \Delta H_{m,cap}\right) / \right.$ $\left.\left(\Delta H_{c,PCM} + \Delta H_{m,PCM}\right)\right]$, where the subscripts c and m are related to crystallization and melting processes, and cap and PCM refer to microcapsules and pure PCM, respectively. The values found for the C14, C18 and paraffin wax-based

microcapsules are 9.1%, 10.6% and 14.8%, respectively. These values are lower than others found in studies in the literature, many of which lack details of how the microcapsules were cleaned, and the presence of PCM on the outside of the microcapsule can falsify some results. Our experience makes us to think that cleaning is a more complicated process than is expected. However, the capsules based on paraffin wax showed the highest encapsulation efficiency.

The isobaric specific heat of the microcapsules prepared and the pure Cu$_2$O in the range 258–353 K was estimated by temperature modulated differential scanning calorimetry as is described above. Figure 13 shows the values obtained. The measurements were performed in triplicate and deviation lower 2% was found in all measurements performed. The discontinuity observed in the values for the microcapsules is due to the phase change. For the pure Cu$_2$O sample, the values are practically constant in the range measured, about 0.35 J g^{-1} K^{-1}, which is verified to be in good agreement compared to values found in the literature, with a maximum relative deviation below 1.7% [26]. The values obtained for the microcapsules based on the three PCMs were higher than those obtained for the pure Cu$_2$O. The values were also
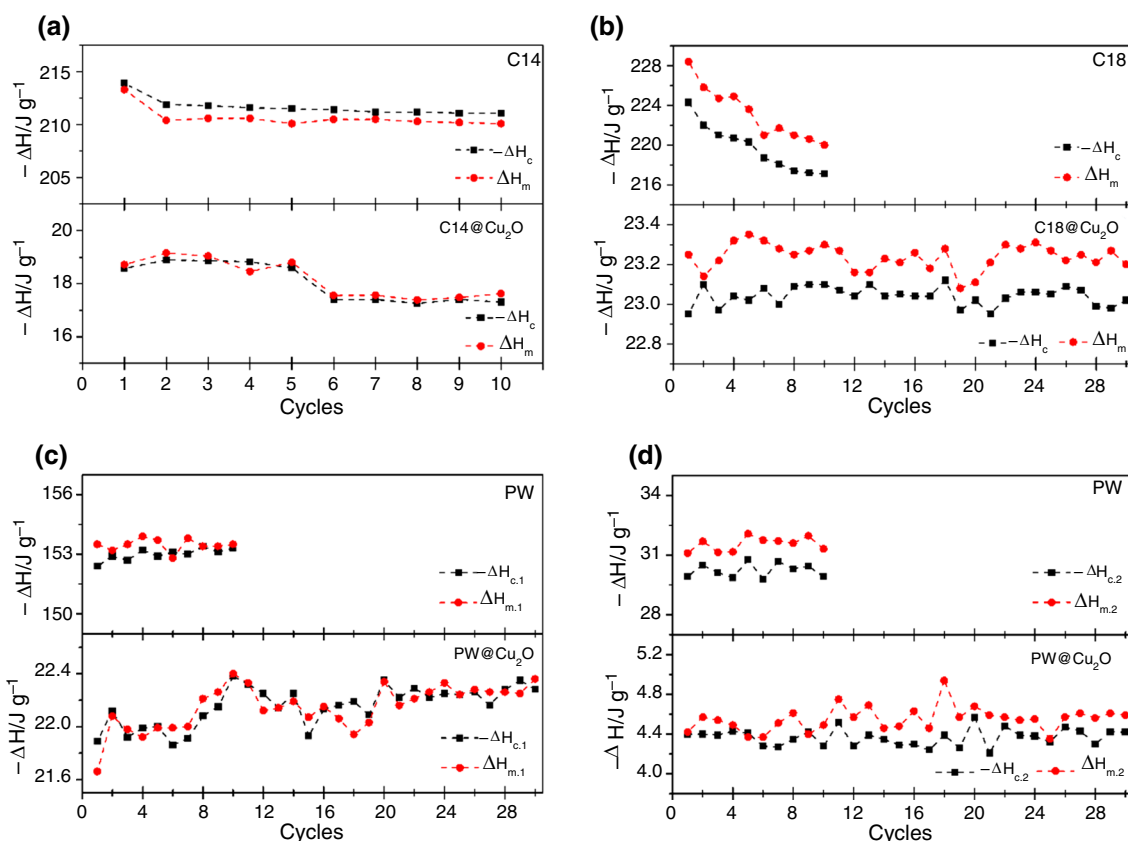
Fig. 12 Melting and crystallization enthalpy values for: **a** pure C14 and C14@Cu$_2$O; **b** pure C18 and C18@Cu$_2$O; and **c** paraffin wax and PW@Cu$_2$O samples
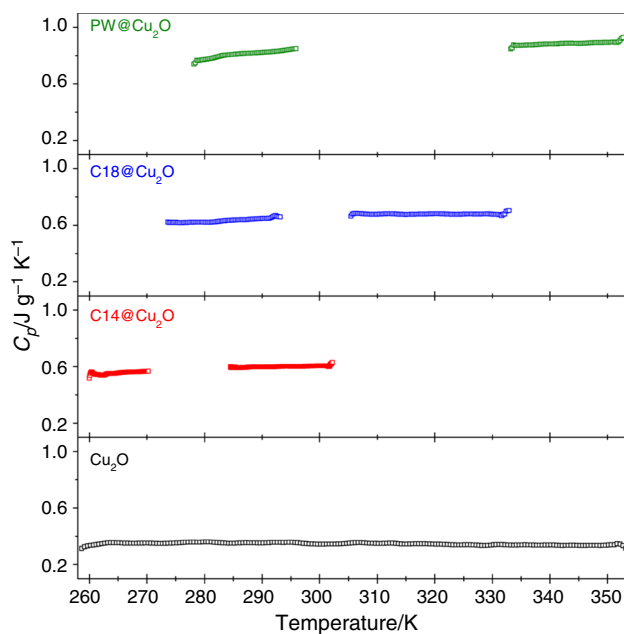
Fig. 13 Isobaric specific heat values for the microcapsules prepared and for the reference sample of Cu$_2$O

higher for the liquid phase than for the solid phase. For the C14 and C18-based microcapsules, the values were practically constant with temperature for each phase. But in the case of the paraffin wax-based microcapsules, the C_P values increased linearly with temperature. For the microcapsules based on C14 and C18, isobaric specific heat values were found of up to 0.62 and 0.68 J g^{-1} K^{-1}, respectively. The highest values were obtained for the microcapsules based on paraffin wax, these reaching 0.85 J g^{-1} K^{-1}, at 78 ºC. These three values mean an increase of about 77%, 94% and 140% compared with the pure Cu$_2$O for the microcapsules based on C14, C18 and paraffin wax. This means microcapsules are able to store more thermal energy than the inorganic material to be used in different applications. In addition, as reported previously [27], the increase in C_P is related with the amount of PCM inside the capsules; thus, these values are in good agreement with the values for the encapsulation efficiency discussed above.

Conclusions

In this study, microcapsules were prepared based on Cu_2O containing different PCMs. The preparation methodology was optimized, and a complete physical and chemical characterization were performed. XRD and XPS confirmed the presence of Cu_2O, while FTIR confirmed the presence of C14, C18 and paraffin wax in the microcapsules prepared. From electron microscopy, the formation of microcapsules with an octahedral morphology was observed, and the presence of the PCMs inside the capsules was confirmed. According to the potential use of the microcapsules as thermal storage systems, their thermal properties were measured. We performed heating/cooling cycles using the differential scanning calorimetry technique, and the values of the melting and crystallization temperature were estimated. We only observed slight differences in the cycles, so we can conclude the microcapsules prepared are highly stable after several heating/cooling cycles. In addition, the melting and crystallization enthalpy were estimated and the efficiency of the encapsulation was calculated, reaching 14.8% for paraffin wax-based microcapsules. Finally, the isobaric specific heat was measured to evaluate the storage capability of the encapsulated PCMs with regard to the pure Cu_2O with a view to their use as thermal storage systems. An increase in the isobaric specific heat of about 140% was found for the microcapsules based on paraffin wax with regard to the pure Cu_2O.

References

1. Fares RL, Webber ME. The impacts of storing solar energy in the home to reduce reliance on the utility. Nat Energy. 2017;2(2):17001. https://doi.org/10.1038/nenergy.2017.1.

2. Aftab W, Huang XY, Wu WH, Liang ZB, Mahmood A, Zou RQ. Nanoconfined phase change materials for thermal energy applications. Energy Environ Sci. 2018;11(6):1392–424. https://doi.org/10.1039/c7ee03587j.

3. Li M, Wu ZS, Tan JM. Properties of form-stable paraffin/silicon dioxide/expanded graphite phase change composites prepared by sol–gel method. Appl Energ. 2012;92:456–61. https://doi.org/10.1016/j.apenergy.2011.11.018.

4. Oro E, de Gracia A, Castell A, Farid MM, Cabeza LF. Review on phase change materials (PCMs) for cold thermal energy storage applications. Appl Energy. 2012;99:513–33. https://doi.org/10.1016/j.apenergy.2012.03.058.

5. Agyenim F, Hewitt N, Eames P, Smyth M. A review of materials, heat transfer and phase change problem formulation for latent heat thermal energy storage systems (LHTESS). Renew Sust Energy Rev. 2010;14(2):615–28. https://doi.org/10.1016/j.rser.2009.10.015.

6. Su WG, Darkwa J, Kokogiannakis G. Review of solid–liquid phase change materials and their encapsulation technologies. Renew Sust Energy Rev. 2015;48:373–91. https://doi.org/10.1016/j.rser.2015.04.044.

7. Hunger M, Entrop AG, Mandilaras I, Brouwers HJH, Founti M. The behavior of self-compacting concrete containing micro-encapsulated phase change materials. Cement Concrete Comp. 2009;31(10):731–43. https://doi.org/10.1016/j.cemconcomp.2009.08.002.

8. Wang Y, Zhao Y, Liu Q, Lei J. Study on a novel solid–solid phase change materials: solvent-free preparation, thermal properties and phase separation behaviors. J Therm Anal Calorim. 2020;141:1305–15. https://doi.org/10.1007/s10973-019-09132-5.

9. Dong X, Mao J, Geng S, Li Y, Hou P, Lian H. Study on performance optimization of sodium sulfate decahydrate phase change energy storage materials. J Therm Anal Calorim. 2021;143:3923–34. https://doi.org/10.1007/s10973-020-09306-6.

10. Dong X, Mao J, Geng S, Zhang Y, Lian H, Hou P. Microencapsulation of sodium sulfate decahydrate composite phase-change energy storage materials. J Therm Anal Calorim. 2022;147:7709–18. https://doi.org/10.1007/s10973-021-11026-4.

11. De Castro PF, Ahmed A, Shchukin DG. Confined-volume effect on the thermal properties of encapsulated phase change materials for thermal energy storage. Chem Eur J. 2016;22(13):4389–94. https://doi.org/10.1002/chem.201505035.

12. Chen Z, Cao L, Shan F, Fang GY. Preparation and characteristics of microencapsulated stearic acid as composite thermal energy storage material in buildings. Energy Build. 2013;62:469–74. https://doi.org/10.1016/j.enbuild.2013.03.025.

13. Belessiotis GV, Papadokostaki KG, Favvas EP, Efthimiadou EK, Karellas S. Preparation and investigation of distinct and shape stable paraffin/SiO2 composite PCM nanospheres. Energy Convers Manag. 2018;168:382–94. https://doi.org/10.1016/j.enconman.2018.04.059.

14. Liang SE, Li QB, Zhu YL, Chen KP, Tian CR, Wang JH, et al. Nanoencapsulation of *n*-octadecane phase change material with silica shell through interfacial hydrolysis and polycondensation

in miniemulsion. Energy. 2015;93:1684–92. https://doi.org/10.1016/j.energy.2015.10.024.

15. Ezhumalai DS, Sriharan G, Harikrishnan S. Improved thermal energy storage behavior of CuO/Palmitic acid composite as phase change material. Mater Today Proc. 2018;5(6):14618–27. https://doi.org/10.1016/j.matpr.2018.03.053.

16. Zheng ZL, Jin JD, Xu GK, Zou JL, Wais U, Beckett A, et al. Highly stable and conductive microcapsules for enhancement of joule heating performance. ACS Nano. 2016;10(4):4695–703. https://doi.org/10.1021/acsnano.6b01104.

17. Zheng ZL, Chang Z, Xu GK, McBride F, Ho A, Zhuola Z, et al. Microencapsulated phase change materials in solar-thermal conversion systems: understanding geometry-dependent heating efficiency and system reliability. ACS Nano. 2017;11(1):721–9. https://doi.org/10.1021/acsnano.6b07126.

18. Wu S, Ma X, Peng D, Bi Y. The phase change property of lauric acid confined in carbon nanotubes as nano-encapsulated phase change materials. J Therm Anal Calorim. 2019;136:2353–61. https://doi.org/10.1007/s10973-018-7906-3.

19. Meng X, Zhang H, Sun L, Xu F, Jiao Q, Zhao Z, et al. Preparation and thermal properties of fatty acids/CNTs composite as shape-stabilized phase change materials. J Therm Anal Calorim. 2013;111:377–84. https://doi.org/10.1007/s10973-012-2349-8.

20. Zhang XX, Song JM, Jiao J, Mei XF. Preparation and photocatalytic activity of cuprous oxides. Sol State Sci. 2010;12:1215–9. https://doi.org/10.1016/j.solidstatesciences.2010.03.009.

21. Borgohain K, Murase N, Mahamuni S. Synthesis and properties of Cu_2O quantum particles. J Appl Phys. 2002;92(3):1292–7. https://doi.org/10.1063/1.1491020.

22. Naumkin AV, Kraut-Vass A, Gaarenstroom SW, Powell CJ. NIST standard reference database 20, Version 4.1. 2012.

23. Biesinger MC, Lau LWM, Gerson AR, Smart RSC. Resolving surface chemical states in XPS analysis of first row transition metals, oxides and hydroxides: Sc, Ti, V Cu and Zn. Appl Surf Sci. 2010;257(3):887–98. https://doi.org/10.1016/j.apsusc.2010.07.086.

24. Fang GY, Li H, Yang F, Liu X, Wu SM. Preparation and characterization of nano-encapsulated *n*-tetradecane as phase change material for thermal energy storage. Chem Eng J. 2009;153(1–3):217–21. https://doi.org/10.1016/j.cej.2009.06.019.

25. Choi J, Fujita H, Ogura M, Sakoda A. Confinement effect on enthalpy of fusion and melting point of organic phase change materials in cylindrical nanospace of mesoporous silica and carbon. Adsorption. 2018;24(4):345–55. https://doi.org/10.1007/s10450-018-9946-1.

26. Lide DR. CRC handbook of chemistry and physics. 90th ed. Boca Raton, Florida: CRC Press; 2009.

27. Qiu XL, Li W, Song GL, Chu XD, Tang GY. Fabrication and characterization of microencapsulated *n*-octadecane with different crosslinked methylmethacrylate-based polymer shells. Sol Energy Mater Sol Cells. 2012;98:283–93. https://doi.org/10.1016/j.solmat.2011.11.018.